

Charging of Submicron Structures during Silicon Dioxide Etching in One- and Two-Frequency Gas Discharges

A. P. Palov^a, Yu. A. Mankelevich^a, T. V. Rakhimova^a, and D. Shamiryan^b

^a Skobeltsyn Institute of Nuclear Physics, Moscow State University, Moscow, 119992 Russia

^b Interuniversity Microelectronics Centre, Kapeldreef 75, B-3001 Leuven, Belgium

Received March 19, 2010

Abstract—A model that combines the Monte Carlo method for calculating electron and ion trajectories in three-dimensional geometry and an analytic approach developed for calculating an electric field in two-dimensional geometry is used to simulate the charging of the surface of periodic submicron SiO₂ structures by electron and ion fluxes in the plasma of a one- and a two-frequency capacitive RF discharge. The energy distribution function of the electrons and ions that come to the bottom of a submicron structure in an argon and an argon-containing plasma is calculated for structures with a width of 11–45 nm and an aspect ratio of $d/w = 1–10$ (where d and w are the depth and width of the structure). It is shown that secondary electron–electron emission plays an important role in the redistribution of the electric charge and, accordingly, of the electric potential in a submicron structure. It is demonstrated that, when the secondary electron–electron emission mechanism is taken into account, the ion energy spectrum at the bottom of a submicron structure is shifted toward lower energies and becomes broader in comparison with the spectrum of an ion flux from an RF discharge plasma. Moreover, the shift and broadening depend only on the secondary electron–electron emission coefficient, the energy of the charged particles, and the aspect ratio.

DOI: 10.1134/S1063780X10100065

1. INTRODUCTION

Numerical simulation provides an important method for studying complex processes that occur during the plasma etching of semiconductors and dielectrics in present-day CMOS technology. The etching process can be described in two steps: the first is the description of the gas-discharge plasma and the second is the description of the interaction of the discharge plasma with the surface of a dielectric or a semiconductor. The latter, which deals immediately with the anisotropic etching of the structures, is governed by the ion-stimulated processes on the dielectric and semiconductor surfaces [1, 2]. The electric charging of the structure surface by charged plasma particles has a great influence on both the etching rate and the shape of the etched structures. On the whole, the surface charging has negative effects, such as nonuniform etching of the bottom and walls of the structure, the termination of etching, or substrate breakdown [3]. The objective of the present paper is to develop physical and numerical models that can give an adequate description of the charging of dielectric structures in a multicomponent multifrequency gas-discharge plasma. In what follows, a submicron structure will be called a trench of depth d and width w .

The first publications on one of the most important problems in CMOS technology—charging of dielectrics—appeared in 1980s, when Yoshida and Watanabe [4] reported dielectric breakdown and

Hashimoto [5, 6] explained this phenomenon. A qualitative explanation of the trench charging is now generally accessible [7]. The main idea is that the plasma ions are incident normally on the dielectric surface, while the plasma electrons, obeying an isotropic velocity distribution, produce a negative charge at the entrance to the trench. The result is that, in the local field of the trench, the ion and electron trajectories become curved toward the trench walls and bottom, respectively. The potential at the surface of the trench becomes steady-state when the ion and electron fluxes on the entire trench surface become the same.

As far as we know, Arnold and Sawin [8] were the first to simulate the charging of an individual dielectric trench by plasma ions (with an energy of 100 eV) and electrons (with a temperature of 4 eV) in two-dimensional (2D) geometry. They solved the problem of how the ion and electron fluxes become the same over the entire trench surface. Since then, a large number of papers have been devoted to studying the steady-state potential at the surface of both dielectric and semiconductor trenches [7–15]. In addition, interest has recently grown in studying the dynamic component of the potential at the surface of nanoscale trenches, and some progress has been achieved in this direction [16, 17]. To the best of our knowledge, however, the charge redistribution in a trench by the secondary electron–electron emission (SEEE) mechanism was not taken into account. A possible reason is that there are no reliable experimental data on the SEEE coefficients

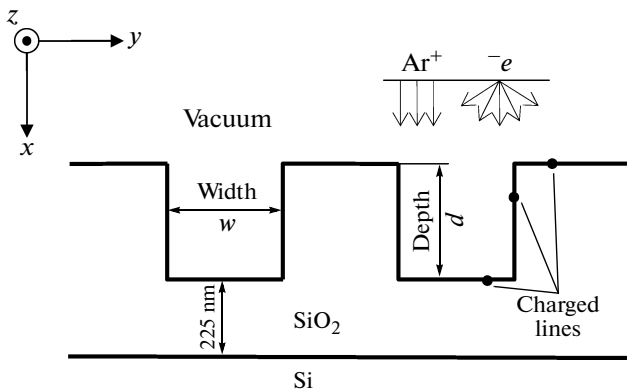


Fig. 1. Schematic of the trenches for which the electric field and potentials were calculated. The trenches are periodic in the y direction and are unbounded in the z direction. The aspect ratio is defined by $AC = d/w$.

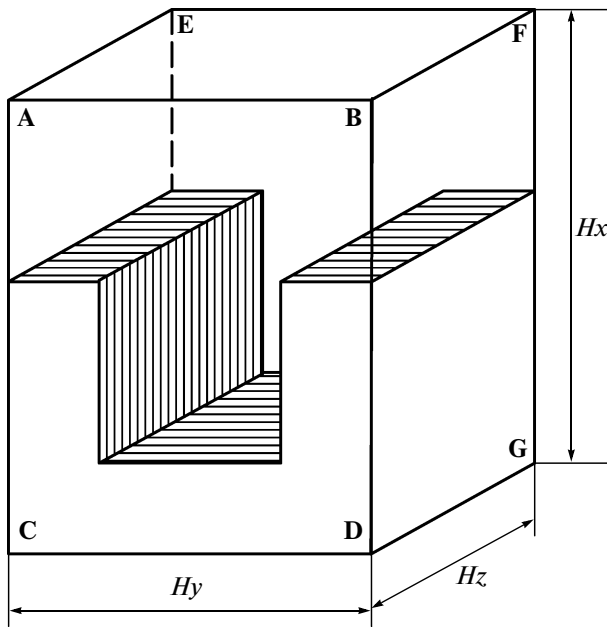


Fig. 2. Computation region in which the trajectories of charged plasma particles in the trenches were simulated.

for dielectrics and semiconductors in the range of low energies of the bombarding electrons (0–50 eV). Thus, the experimental data on the SEEE coefficients for silicon dioxide were for a long time known only for electron energies above 50 eV [18]. Dunaevsky et al. [19] bridged this gap, and we were then able to describe charge redistribution in silicon dioxide trenches with allowance for the SEEE mechanism. Our present work is aimed at simulating trench charging in the plasma of one- and two-frequency capacitive RF discharges with allowance for the electrons reflected inelastically from the trench surface and cascade electrons escaping

from the latter. We also analyze the possible effect of the secondary ion–electron emission (SIEE) mechanism on the trench charging process.

In Section 2, we describe the physical model and numerical scheme for the charging of periodic trenches with different aspect ratios in a one- and a two-frequency multicomponent gas-discharge plasma. In Section 3, we present the results of calculating the ion and electron energy spectra at the bottom of the trenches and the electric potential within the trenches and also discuss the results. In the Conclusions, a summary of our work is given.

2. PHYSICAL MODEL

Figure 1 shows the geometry of the trenches under investigation. The trenches are periodic in the y direction and are unbounded in the z direction. For simplicity, the trenches are assumed to have the same shape along the z axis, an assumption that makes the problem of calculating the electric field two-dimensional. In this case, each point on the trench surface corresponds to an infinitely long line in the z direction. The linear charge density along the lines is calculated from the coordinates of the ions and electrons deposited on the three-dimensional (3D) trench surface. The trajectories of charged particles were simulated in the 3D region shown in Fig. 2. Periodic boundary conditions were imposed at sides ABCD and BDGF and their opposite sides.

The values of the ion and electron fluxes at boundary ABFE in Fig. 2 were taken from [20, 21], and their choice depended on the problem to be solved. Numerical simulations were carried out for a one- and a two-frequency RF discharge in argon and an $Ar/CF_4/N_2$ mixture. The total electric charge in the computation region was always maintained to be zero. The electron energy distribution function at the entrance to the computation region was assumed to be Maxwellian with a temperature of 2–4 eV, and the angular electron velocity distribution was assumed to be isotropic. The ion energy distribution was described by a delta function with an energy of 170 eV for a one-frequency plasma and by the calculated values from [20, 21] for a two-frequency plasma. It was also assumed that the ion velocity vector was directed along the normal to the trench surface. The deviations of the vector from the normal were described by a Gaussian distribution with a mean deviation of 2° .

The values of the external electric fields of an RF discharge plasma were taken from [20, 21]. The coefficient of SIEE from a silicon dioxide surface, equal to 0.005–0.02 [22] and 0.5 [23], is substantially smaller than the SEEE coefficient, equal to 1–1.5 [18, 19]. However, we also analyzed the effect of the SIEE mechanism on the formation of the potential at the trench bottom.

We have no experimental data for the reflection coefficient of argon ions from a silicon dioxide surface, so in order to estimate this coefficient, we used the reflection coefficient of argon ions from a silicon surface. Since this latter coefficient is smaller than 0.2% [24], we ignored the ion reflection mechanism in our simulations.

The distance between plane ABFE and the upper trench surface was chosen to be the trench depth, because, in this case, the electric field of the trench has a negligible effect on the starting ions and electrons. Test calculations showed that the solutions are stable up to distances of one-third of the trench depth. The distance between the silicon dioxide surface and the trench bottom was set equal to 225 nm, a value that is typical of present-day etching experiments.

The plasma within the trench was assumed to be collisionless, because, in the discharges under study, the mean free path of the charged particles certainly exceeds the trench sizes. It was also assumed that, in silicon dioxide, there are no loss currents.

In order to hasten the calculation of the electric field generated by the charges deposited on the trench surface, we set the permittivity of the medium in the entire computation region equal to that of vacuum. In this case, for a system of periodic trenches, the 2D electric field can be calculated analytically [16], an approach that allowed us to rapidly obtain qualitative estimates on a personal computer without pretending to calculate exact quantitative results. In what follows, we present analytic formulas for the electric field and potential and correct the misprints made in the corresponding formulas in [16].

2.1. Analytic Calculation of the 2D Electric Field in Periodic Trenches

In Gaussian coordinates, the 2D electric field created at an arbitrary point by an infinitely long line that

lies on the trench surface and is parallel to the z axis can be written as

$$\mathbf{E} = \frac{2\chi\mathbf{r}}{\varepsilon r^2}, \quad (1)$$

$$\chi = \frac{q}{H_z},$$

where χ is the linear charge density on the line, \mathbf{r} is the shortest distance from an arbitrary spatial point within the trench to the line, $\varepsilon = 1$ is the permittivity of the medium, and q is the charge deposited on the trench surface. For N lines on the trench surface and for n trenches, the x and y components of the electric field produced at an arbitrary point (x, y) are expressed as

$$E_x(x, y) = \sum_{j=1}^N \frac{2\chi_j}{\varepsilon} \sum_{n=-\infty}^{\infty} \frac{x - x_j}{r^2}, \quad (2)$$

$$E_y(x, y) = \sum_{j=1}^N \frac{2\chi_j}{\varepsilon} \sum_{n=-\infty}^{\infty} \frac{y - (y_j + nH_y)}{r^2},$$

where $r^2 = (x - x_j)^2 + (y - (y_j + nH_y))^2$ and (x_j, y_j) are the coordinates of the j th line. Summing expressions (2) over n yields

$$E_x(x, y) = \sum_{j=1}^N \frac{2\chi_j}{\varepsilon H_y} \frac{\sinh(2\pi(x - x_j)/H_y)}{[\cosh(2\pi(x - x_j)/H_y) - \cos(2\pi(y - y_j)/H_y)]}, \quad (3)$$

$$E_y(x, y) = \sum_{j=1}^N \frac{2\chi_j}{\varepsilon H_y} \frac{\sin(2\pi(y - y_j)/H_y)}{[\cosh(2\pi(x - x_j)/H_y) - \cos(2\pi(y - y_j)/H_y)]}.$$

The corrections of the electric field components, ΔE_x , ΔE_y , due to the image charges induced in the conducting substrate are given by the same formulas (3) with the replacement $x_j \rightarrow x_j + 2b_j$, where b_j is the distance from the j th line to the substrate. The resulting electric potential at an arbitrary point (x, y) has the form

$$\phi(x, y) = -\sum_{j=1}^N \frac{\chi_j}{\varepsilon \pi} \ln \left\{ \frac{[\cosh(2\pi(x - x_j)/H_y) - \cos(2\pi(y - y_j)/H_y)]}{[\cosh(2\pi(x - (x_j + 2b_j))/H_y) - \cos(2\pi(y - y_j)/H_y)]} \right\} + \text{const.} \quad (4)$$

The arbitrary constant was chosen so that the potential at the central point of plane ABFE in Fig. 2 was zero. The electric field and potential were calculated from formulas (3) and (4) on a 400×60 spatial mesh. The electric field at an arbitrary point of the computation region was calculated by linear interpolation. The matrices of the electric field components

were recalculated every time when each next charge was deposited on the trench surface.

2.2. Accounting for the SEEE Processes

The deposition of plasma ions and electrons on trench surfaces was simulated in different ways. The ion trajectories were traced until they came into con-

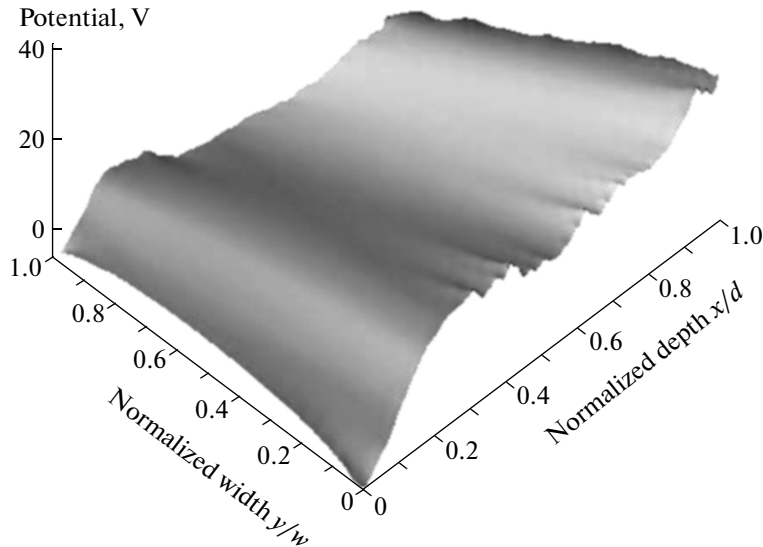


Fig. 3. Electric potential within a trench with $AC = 5\ 0.124$ s after the beginning of plasma etching, calculated with allowance for the SEEE mechanism.

tact with the trench surface and the coordinates of the contact points were stored in the computer memory. In contrast, depending on its energy and its angle of incidence on the trench surface, each of the electrons can either rest on the surface or produce k secondary electrons with the most probable energy ε_i . In the last case, the trench surface was assigned the $k - 1$ positive charge. The angular distribution of the secondary electrons was assumed to be isotropic.

The number of secondary electrons so produced was determined based on the SEEE coefficient $\sigma = \delta + \eta$, where δ is the coefficient of emission of electrons with energies lower than 15 eV and η is the inelastic reflection coefficient, characterizing the reflection of higher energy electrons. The SEEE coefficient $\sigma(E, \theta) = \sigma_0(E)f(\theta)$ depends on the energy of the primary electron and its angle of incidence relative to the normal to the trench surface. For the coefficient of SEEE from quartz at the normal incidence of an electron beam, $\sigma_0(E)$, we used the experimental data from [18, 19]. Because of the lack of experimental data for $\sigma_0(E)$ in the primary electron energy range 0–10 eV, linear interpolation was used. The angular dependence of the SEEE coefficient was calculated from the formulas

$$f(\theta) = \begin{cases} \cos^{-1.3}\theta, & \theta < 80^\circ, \\ \cos^{-1.3}80^\circ \frac{(90^\circ - \theta)}{(90^\circ - 80^\circ)}, & \theta > 80^\circ, \end{cases} \quad (5)$$

where θ is the angle of incidence of a primary electron relative to the trench surface. The first of formulas (5) was obtained from experimental data [25]. Unfortunately, we failed to find experimental values of the

SEEE for electrons the angles of incidence of which are greater than 80° . This is why, the second of formulas (5) is based on the assumption that an electron flying along the surface of a dielectric neither interacts with it nor produces secondary electrons. When the energy of an electron became higher than the width of the forbidden zone for SiO_2 , 8.9 eV, the onset of a secondary electron with the probability $\sigma(E, \theta)$ was simulated. In the opposite case, an incident electron was either reflected elastically from the trench surface or was deposited there.

We did not take into account the actual distribution of the charge within the dielectric and its relaxation in the electric field, as well as the actual angular and energy distributions of the secondary electrons escaping from the dielectric. Of course, all these factors can influence the formation of the electric potential on the trench surface, and they will be accounted for in a more complicated version of the model in which the electron trajectories within SiO_2 will be traced by the Monte Carlo method, a way in which more exact quantitative results are to be obtained.

3. DISCUSSION OF THE RESULTS

The charged particle trajectories, electric field, and electric potential within silicon dioxide trenches were simulated by the MOTREV (Modeling of Trench Evolution) computer code, which we developed at the Department of Microelectronics, Skobeltsyn Institute of Nuclear Physics, Moscow State University.

We calculated charged particle fluxes in the multi-component plasma of a one- and a two-frequency capacitive RF discharge for trenches with a width of

11–45 nm and an aspect ratio ($AC = d/w$) in the range $1 \leq AC \leq 10$. Our numerical simulations showed that the potentials and the ion and electron energy spectra at the bottom of trenches of constant aspect ratio are independent of the trench width. This is why we present here only the results obtained for 45-nm-wide trenches.

Calculations of the ion energy spectra for the chosen values of the charged particle flux and aspect ratio AC show that the positions of the peaks in the spectra and their width are stable on time scales longer than 0.06 s; i.e., a steady-state potential on the trench bottom forms essentially instantaneously, during several tens of milliseconds. For the chosen values of the ion and electron fluxes, this corresponds to the etching of one atomic layer at a mean rate of 1 nm/s.

Figure 3 shows a representative relief of the potential obtained by simulating the interaction of a plasma containing 170-eV ions and 3.4-eV electrons with the surface of a silicon dioxide trench. The potential relaxes to a quasi-steady state after about ≈ 0.1 s of plasma etching. The interaction of electrons with the trench surface was simulated with allowance for the SEEE mechanism. In Fig. 3, we can distinguish three characteristic regions of the potential: the first region, where the potential is slightly negative, is at the entrance to the trench; the second region is a positive hump immediately after the first region; and the third region resembles a plateau of gradually increasing height. A detailed description of the mechanisms responsible for the formation of the three different regions of the potential was given in our earlier paper [26].

The goal of our present work is to demonstrate the effect of the SEEE mechanism on the formation of a quasi-steady potential within a silicon dioxide trench and on the ion and electron energy spectra at the trench bottom in both a one- and a two-frequency capacitive RF discharge.

Figure 4 displays the electric potential at the symmetry axis of the trench, calculated for a one-frequency 81-MHz discharge in argon for different values of the coefficient of attenuation of the SEEE mechanism. A zero attenuation coefficient indicates that the SEEE mechanism was ignored in simulations. An attenuation coefficient equal to unity corresponds to the experimental value of the SEEE coefficient for silicon dioxide. We can see from Fig. 4 that a substantial decrease in the SEEE coefficient (e.g., by a factor of 2 to 3) leads to a proportional decrease in the potential at the bottom of the trench. Hence, even if the experimental data on the SEEE coefficient are highly unrealistic, the values of the potential at the trench bottom that are calculated here differ strongly from the generally accepted ones, which were obtained from numerical simulations of trench charging without allowance for the SEEE mechanism.

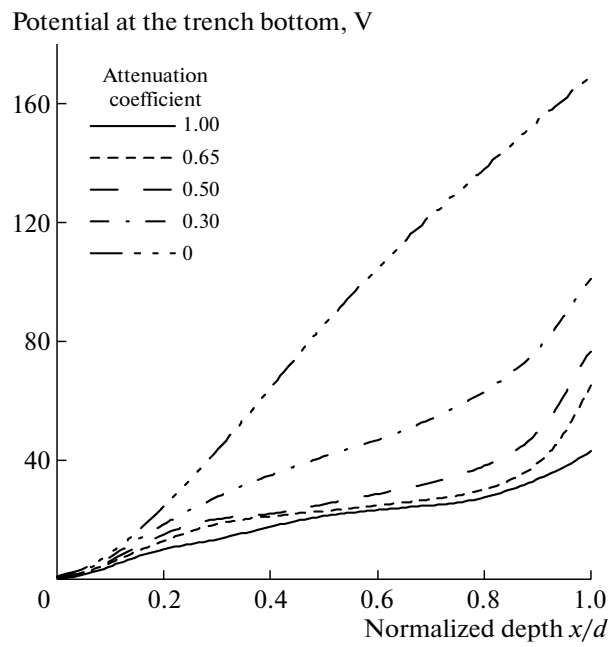


Fig. 4. Electric potential at the symmetry axis of a trench with $AC = 5$, calculated as a function of the trench depth for different values of the coefficient of attenuation of the SEEE mechanism.

Figure 5 shows how the ion energy spectrum at the bottom of the trench varies with variation in the potential in Fig. 4. From Fig. 5 we can see that an increase in the potential at the trench bottom naturally leads to an appreciable shift of the peak in the spectrum toward lower energies. For a zero attenuation coefficient, the ion spectrum is a delta function that is peaked at the energy of thermalized ions and has a width of several electronvolts due to nonstationary potential fluctuations. Such a radical variation of the ion energy distribution function at the trench bottom shows that the model in which the SEEE mechanism is ignored predict very unrealistic probabilities of the ion-induced etching.

Figure 6 shows the electric potential at the symmetry axis of the trench in a one-frequency 80-MHz discharge in argon, calculated with allowance for the SEEE mechanism for different values of the SIEE coefficient. We can see that variations in the SIEE coefficient over a wide range from 0 to 0.5 lead only to slight potential fluctuations at the trench bottom in the range 2–5 V. The corresponding variations in the ion energy spectrum at the bottom of the trench are presented in Fig. 7. Based on the results of these simulations, we can suppose that the SIEE mechanism has an insignificant impact on the formation of the potential at the trench bottom.

Along with the SEEE coefficient and electron-to-ion energy ratio, the aspect ratio is the main parameter governing the potential amplitude at the trench bot-

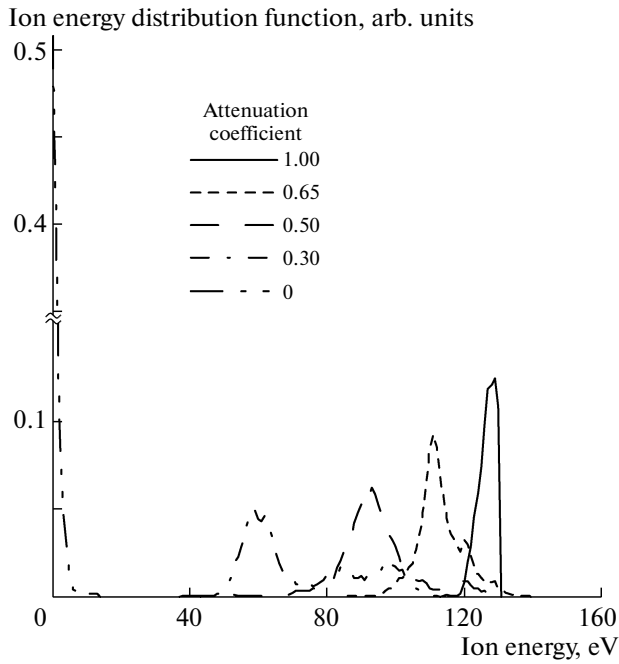


Fig. 5. Ion energy spectrum at the bottom of a trench with $AC = 5$, calculated for different values of the coefficient of attenuation of the SEEE mechanism and averaged over the last 0.06 s of etching.

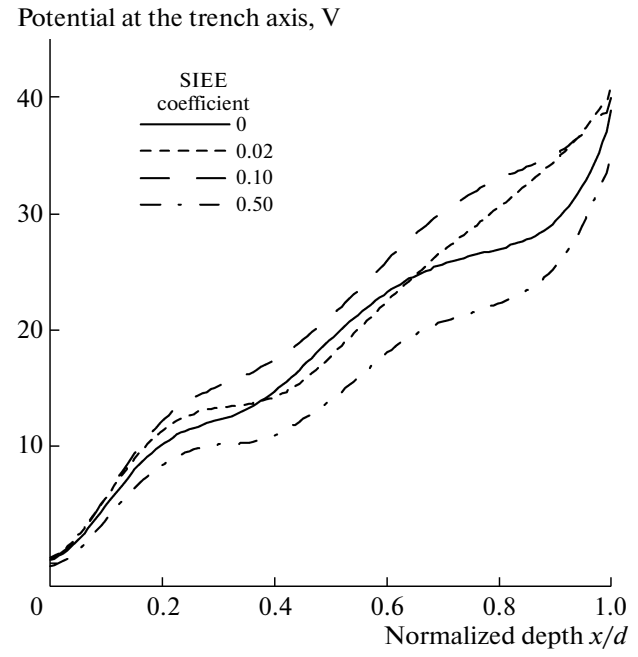


Fig. 6. Electric potential at the symmetry axis of a trench with $AC = 5$, calculated with allowance for the SEEE mechanism for different values of the SIEE coefficient.

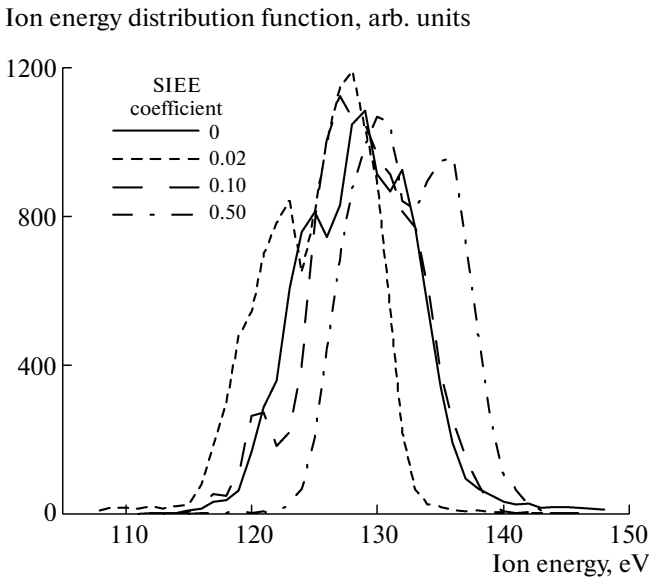


Fig. 7. Ion energy spectrum at the bottom of a trench with $AC = 5$, calculated for different values of the SIEE coefficient and averaged over the last 0.06 s of etching.

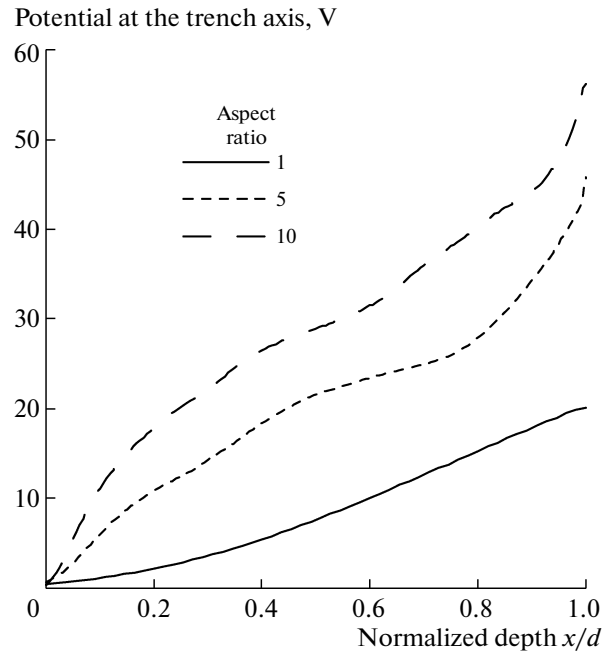


Fig. 8. Electric potential at the trench axis, calculated with allowance for the SEEE mechanism for different values of the aspect ratio.

tom. Figure 8 shows the electric potential at the trench axis, calculated with allowance for the SEEE mechanism for different values of the aspect ratio. It can be clearly seen that, at the trench bottom ($x/d = 1$), the

quasi-steady potential increases from 20 V for $AC = 1$ to 60 V for $AC = 10$. This is explained by the fact that the number of electrons lost at the trench walls increases with increasing AC .

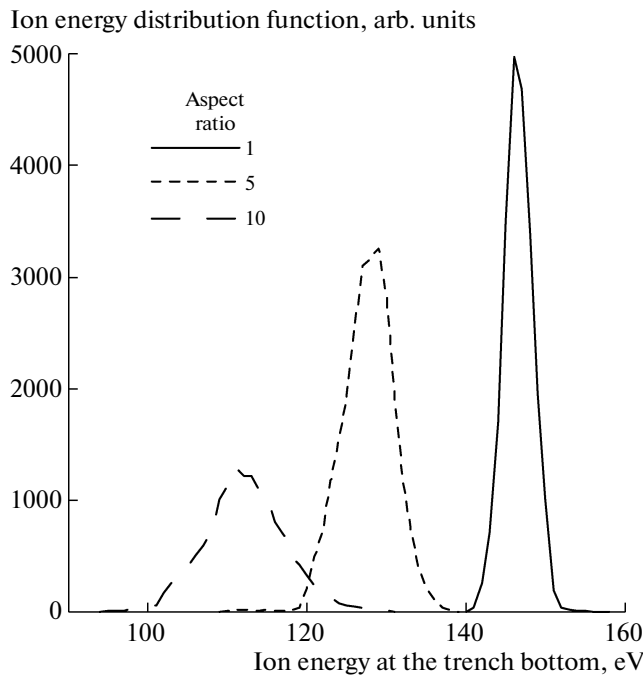


Fig. 9. Ion energy spectrum calculated with allowance for the SEEE mechanism for different values of the aspect ratio and averaged over the last 0.06 s of etching.

Figure 9 shows ion energy spectra at the bottom of a trench with different aspect ratios AC . The shift of the peak, by about 23 eV = 170–147 eV, and the width of the spectrum, about ≈ 12 eV, are minimum for $AC = 1$. The situation with the spectrum for $AC = 10$ is oppo-

site: the peak is shifted relative to an energy of 170 eV to the maximum extent and has a maximum width of about ≈ 25 eV. The shift in the peak stems from an increase in the steady-state potential at the bottom of the trench. The explanation of the broadening of the spectrum is twofold: first, the nonuniformity of the potential at the trench bottom and, second, the unsteady potential fluctuations during the time interval over which the ion energy spectrum is averaged. As the aspect ratio AC increases (e.g., up to 10), the relative amount of ions and electrons that reach the trench bottom decreases by an order of magnitude, an effect that can considerably influence the dynamics of the potential, because each next charged particle that comes to the bottom contributes markedly to the formation of the charge balance.

In order to give a clearer insight into the formation of the potential at the trench bottom, we calculated the amount of electrons that do not collide with the walls of the trench and reach its bottom (we call such electrons ballistic) as a function of the aspect ratio AC . This dependence allows us to understand what are the values of AC at which the formation of the potential at the bottom is governed primarily by the ballistic electrons and what are those at which the governing role is played by the inelastically reflected and secondary electrons. Figure 10 shows the calculated energy spectra of the electrons that reach the bottom of a trench with $AC = 1$ (solid curve) and $AC = 5$ (dashed curve). Knowing the potential at the trench bottom (see Fig. 8), we can infer that spectral regions $B(AC = 1)$ and $B(AC = 5)$ describe the distribution function of the ballistic electrons. It should be noted that, in these

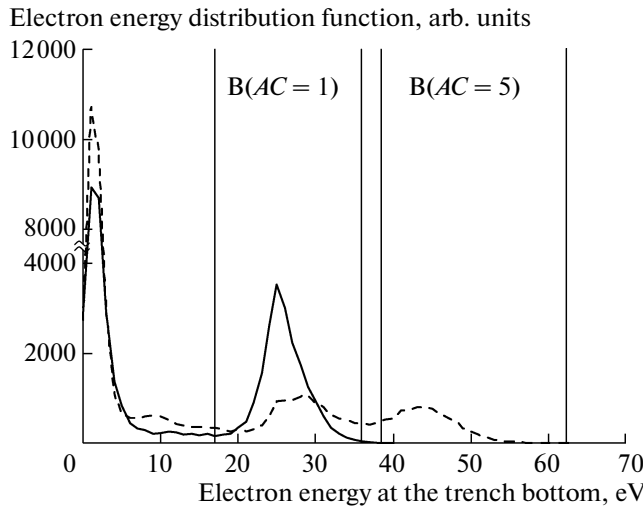


Fig. 10. Energy spectra of the electrons that reach the bottom of a trench with an aspect ratio of 1 (solid curve) and 5 (dashed curve). Regions $B(AC = 1)$ and $B(AC = 5)$ show the spectra of the bottom electrons for $AC = 1$ and $AC = 5$, respectively.

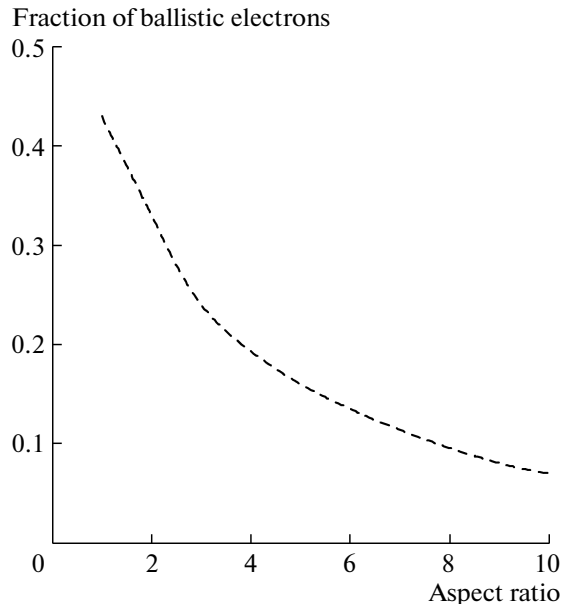


Fig. 11. Fraction of plasma electrons that come to the bottom of the trench without colliding with its walls.

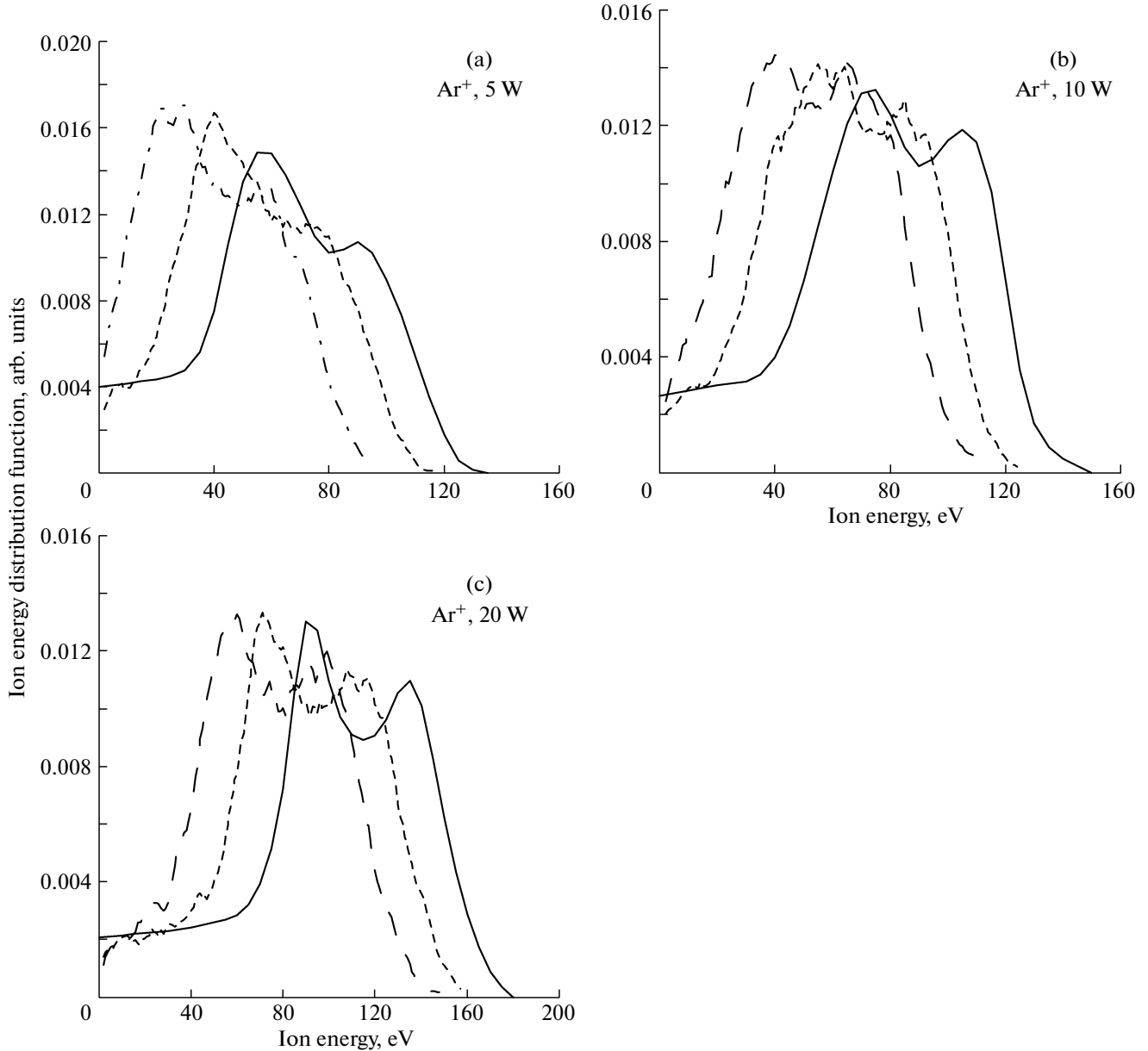


Fig. 12. Ion energy distribution functions calculated for a two-frequency discharge with a power of (a) 5, (b) 10, and (c) 20 W at the higher frequency in a plasma (solid curves) [20] and at the bottom of a trench with $AC = 1$ (dashed curves) and $AC = 5$ (dashed-and-dotted curves).

regions, there also are electrons reflected elastically from the wall just near the entrance to the trench, but the contribution of these electrons is negligibly small. In order to calculate the relative amount of ballistic electrons, we integrated the total energy spectrum of the electrons that reach the trench bottom and the spectrum of the ballistic electrons for each AC value and found the ratio of the results. Calculations of the relative amount of ballistic electrons as a function of the aspect ratio AC are illustrated in Fig. 11. For $AC = 1$, the amount of ballistic electrons is approximately equal to the amount of electrons that have interacted with the trench walls. In contrast, for $AC = 10$, the

contribution of the SEEE mechanism to the formation of the potential at the trench bottom is an order of magnitude greater than that of the ballistic electrons.

Numerical simulations of the charging of trenches with different aspect ratios AC by the plasma of a one-frequency capacitive discharge enabled us to understand the role of SEEE, as well as of the ion energy, in the formation of the energy spectra of the ions that reach the trench bottom. In recent years, the discharges that have been most widely used for high-precision anisotropic etching of submicron structures are capacitive RF discharges in which, under certain two-

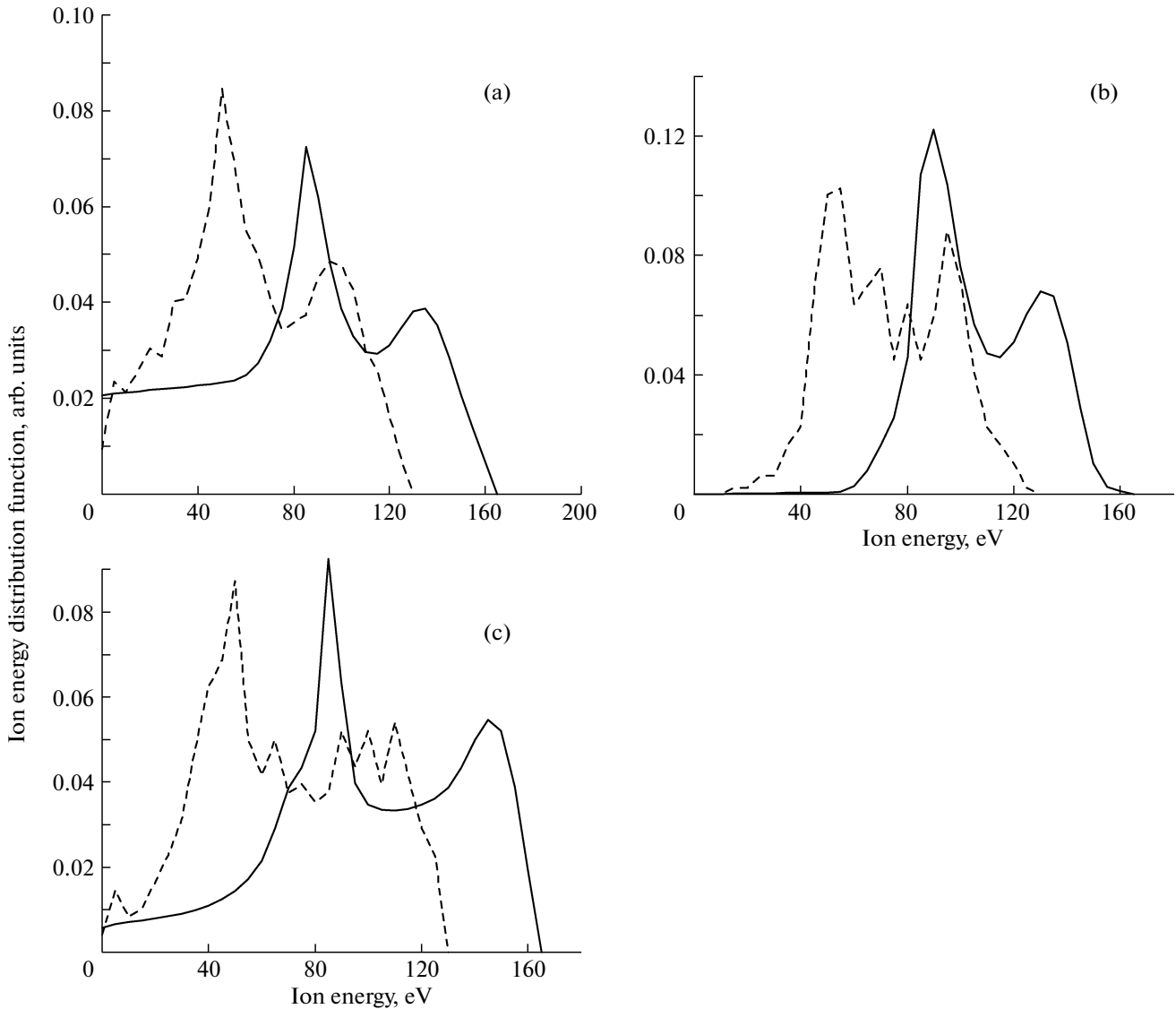


Fig. 13. Distribution functions of (a) Ar^+ , (b) CF_3^+ , and (c) N_2^+ ions in a plasma (solid curves) and at the bottom of a trench with $AC = 5$ (dashed curves).

frequency conditions, the two frequencies play distinctly different roles: the higher one governs the ion flux, and the lower one, the ion energy. The characteristic features of the formation of the ion energy distribution in such a discharge plasma were described in [20, 21]. Accordingly, in analyzing the ion-stimulated etching processes, it is of interest to study the ion energy spectra at the bottom of a trench in two-frequency discharges in Ar and its mixtures with CF_4 and N_2 working gases.

Figure 12 displays the energy distribution functions of Ar^+ ions in a two-frequency discharge plasma (solid curves) and at the bottom of a trench with $AC = 1$ (dashed curves) and $AC = 5$ (dashed-and-dotted curves). The distribution functions of Ar^+ ions bombarding the surface under processing and the temper-

ature of the electrons coming to the working surface, equal to 4.2 eV, were taken from [20], where they were calculated by the particle-in-cell-Monte Carlo (PIC-MC) method—a combination of PIC and MC simulations—for a pressure of 20 mTorr, a discharge input power of 1 W at a frequency of 1.7 MHz and of 5, 10, and 20 W at a frequency of 81 MHz. The width of the plasma layer was calculated to be 0.33 mm, and the density of the ion flux to the working surface was 10^{15} particle/($\text{cm}^2 \text{s}$).

Numerical results show that, at input powers of 5, 10, and 20 W, the ion energy spectra are shifted toward lower energies by about 20 eV for $AC = 1$ and by about 40 eV for $AC = 5$.

Figure 13 shows the energy distribution functions of Ar^+ , CF_3^+ , and N_2^+ ions above the surface under processing (solid curves) and at the bottom of a trench with $AC = 5$ (dashed curves) in a plasma in a 10% CF_4 –10% N_2 –80% Ar mixture, which is often used for ion-stimulated etching. The distribution functions of the ions bombarding the working surface and the electron temperature, equal to 3.4 eV, were taken from [21], where they were calculated by the PIC–MC method for a voltage of 100 V at a frequency of 2 MHz and of 200 V at a frequency of 60 MHz, an electrode sheath of width 0.33 mm, and an ion flux with a total density of 1.3×10^{15} particles/(cm^2 s). In Fig. 13, we also see that, for $AC = 5$, the energy spectrum of all the ions is synchronously shifted toward lower energies by an amount equal to the mean steady-state potential at the trench bottom. The energy spectrum of argon ions is essentially the same as that obtained in [20]. The energy spectra of CF_3^+ and N_2^+ ions differ insignificantly from those calculated for pure argon, a difference that is explained by the difference in the masses of the ions under study.

4. CONCLUSIONS

We have investigated the charging of SiO_2 trenches with a width of 11–45 nm and an aspect ratio of 1–10 by a gas-discharge plasma and analyzed how the electric potential and the ion energy spectra at the bottom of a trench depend on the trench's aspect ratio, the initial energy spectra of the plasma ions and electrons, and secondary electron emission due to the bombardment of the trench by electrons and ions (SEEE and SIEE, respectively). We have described numerical simulations of the spectra of charged particle fluxes typical of the plasma of a one- and a two-frequency low-pressure capacitive RF discharge. We have presented only the numerical results obtained for a trench width of 45 nm, because, for the energies of charged plasma particles chosen for computations, the potential at the trench bottom depends solely on the aspect ratio.

We have shown that the SEEE mechanism should be taken into account in calculating the potential and ion energy spectra at the trench bottom, because the inelastically reflected electrons, as well as the secondary electrons from the trench walls, have a great impact on the charge redistribution in the trench. The electric potentials and ion energy spectra calculated in the present paper differ qualitatively from those obtained based on traditional approaches (in which SEEE and SIEE are ignored). We have also shown that accounting for the SIEE mechanism does not significantly change the ion energy spectra at the trench bottom.

Our analysis of the electron energy spectra in a one-frequency discharge in argon shows that, for $AC =$

1, the amount of ballistic electrons is approximately equal to the amount of electrons interacting with the trench walls and that, for larger aspect ratios in the range $1 \leq AC \leq 10$, the amount of ballistic electrons is an order of magnitude smaller. It is therefore obvious that, already for $AC \approx 3$ –5, the SEEE mechanism dominates the formation of the electron flux to the trench bottom.

That the calculated potential in the trench is stable against small variations in the SEEE coefficient was demonstrated using a trench with the aspect ratio $AC = 5$ as an example.

We have found that, for the chosen values of the fluxes and energies of charged plasma particles, the potential at the trench bottom relaxes to a quasi-steady state for a time equal to 10^7 higher frequency periods (in our case, during a time interval of 0.06 s), which corresponds approximately to the time of etching of one atomic layer of a dielectric.

We have calculated the ion energy distribution functions at the trench bottom from the known charged particle fluxes from the plasma of a two-frequency discharge in Ar and an Ar/ CF_4 / N_2 mixture. In the first case, we have investigated how the initial energy distribution function of argon ions varies in a trench with an aspect ratio of 1 and 5 and a higher frequency power of 5, 10, and 20 W. The results of simulations show that the energy spectrum of plasma ions is shifted by 20 and 40 eV toward lower energies for $AC = 1$ and 5, respectively.

Our analysis of the variation in the spectra of a multicomponent plasma shows that the energy spectrum of all the ions is synchronously shifted toward lower energies, a result that should substantially influence the rates of ion-stimulated reactions at dielectric surfaces.

ACKNOWLEDGMENTS

We are grateful to O.V. Proshina and D.G. Voloshin for providing us with the calculated results for the ion and electron fluxes from the plasma of a two-frequency capacitive RF discharge to the working surface of a dielectric. This work was carried out under the Agreement between Moscow State University and the Interuniversity Microelectronics Centre (Leuven, Belgium) and was supported in part by the Russian Foundation for Basic Research (project no. 08-02-00465), the Key Science School (grant no. SS-3322.2010.2), the RF Agency for Science and Innovations (state contract no. 02.740.11.0235), and the European Network (EU-NET).

REFERENCES

1. D. Zhang and M. Kushner, *J. Appl. Phys.* **87**, 1060 (2000).
2. D. Economou, *Thin Solid Films* **365**, 348 (2000).

3. T. Yagisawa, K. Maeshige, T. Shimada, and T. Makabe, IEEE Trans. Plasma Sci. **32**, 90 (2004).
4. Y. Yoshida and T. Watanabe, in *Proceedings of the 5th Symposium on Dry Process, Tokyo, 1983*, p. 4.
5. K. Hashimoto, Jpn. J. Appl. Phys. **32**, 6109 (1993).
6. K. Hashimoto, Jpn. J. Appl. Phys. **33**, 6013 (1994).
7. W. Hitchon, *Plasma Processes for Semiconductor Fabrication* (Cambridge Univ. Press, Cambridge, 1999).
8. J. C. Arnold and H. H. Sawin, J. Appl. Phys. **70**, 5314 (1991).
9. S. Fang and J. McVittie, IEEE Trans. Electron Dev. **41**, 1034 (1994).
10. T. Kinoshita, M. Hane, and J. P. McVittie, J. Vac. Sci. Technol. B **14**, 560 (1996).
11. G. S. Hwang and K. P. Giapis, Appl. Phys. Lett. **71**, 1945 (1997).
12. U. Kortshagen, J. Vac. Sci. Tech. A **16**, 300 (1998).
13. M. Converse, IEEE Trans. on Plasma Sci. **27**, 1441 (1999).
14. J. Matsui, K. Maeshige, and T. Makabe, J. Phys. D **34**, 2950 (2001).
15. B. Radjenovic, M. Radmilovic-Radjenovic, and Z. Lj. Petrovich, Mater. Sci. Forum **555**, 53 (2007).
16. T. Lee, S. Kim, Y. Jho, et al., Phys. Plasmas **14**, 10350 (2007).
17. J. A. Kenney and G. S. Hwang, J. Appl. Phys. **101**, 044307 (2007).
18. G. Dionne, J. Appl. Phys. **46**, 3347 (1975).
19. A. Dunaevsky, Y. Raitses, and N. J. Fish, Report No. PPPL-3787 (Princeton Plasma Physics Laboratory, Princeton, 2003).
20. T. V. Rakhimova, O. V. Braginsky, V. V. Ivanov, et al., IEEE Trans. Plasma Sci. **34**, 867 (2006).
21. V. Georgieva, PhD Thesis, Antwerpen, 2005.
22. H. K. Kim, T. S. Kim, J. Lee, and S. K. Jo, Phys. Rev. B **76**, 165434 (2007).
23. J. P. Booth, G. Curley, D. Marić, and P. Chabert, Plasma Sources Sci. Technol. **19**, 015005 (2010).
24. H. D. Hagstrum, Phys. Rev. **123**, 758 (1961).
25. H. Seiler, J. Appl. Phys. **54**, R1 (1983).
26. A. P. Palov, Yu. A. Mankelevich, T. V. Rakhimova, and D. Shamiryan, J. Phys. D **43**, 075203 (2010).

Translated by I.A. Kalabalyk